The role of the topset slope in autogenically controlling avulsion and bifurcation timescales in river deltas

O.A. Prasojo[1*], T. B. Hoey[2], A. Owen[1] and R. Williams[1]

[1]School of Geographical and Earth Sciences, University of Glasgow, University Avenue, Glasgow, G12 8QQ, United Kingdom, o.prasojo.1@research.gla.ac.u Amanda.Owen@glasgow.ac.uk, Richard.Williams@glasgow.ac.uk

[2]Department of Civil and Environmental Engineering, Brunel University London, Uxbridge, UB8 3PH, United Kingdom, Trevor.Hoey@brunel.ac.uk

Highlights

- Autogenic interaction of avulsions and bifurcations in delta building processes are investigated through a numerical model
- Delta topset slope serves as the first-order control of autogenic avulsion
- Avulsion and bifurcation can occur simultaneously in river deltas even though they are mechanistically different processes
- Integration with natural system topset slope-avulsion timescales show consistency with our model

Abstract

River deltas are under external stress from sea-level rise, subsidence, and decreases in sediment and water discharges caused by anthropogenic activity. Naturally, delta channels respond to these stressors by avulsing and bifurcating. Avulsion involves an abrupt change of channel course that changes the locus of sediment deposition. Bifurcation occurs in the most seaward parts of river deltas where channels divide due to mouth bar deposition. However, how avulsion (top-down) and bifurcation (bottom-up) processes interact in river deltas is poorly understood. We conducted a suite of morphodynamic numerical model experiments using six scenarios with different slopes, selected within the range observed in natural deltas, upstream from the delta apex. The experiments allow us to understand the internal (autogenic) interaction of avulsion and bifurcation in the absence of external (allogenic) forcing. We find that topset slope

(S_{topset}) primarily controls the avulsion timescale (T_a) with $T_a = 0.3S_{topset}^{-1.18}$ ($R^2 = 69\%$; $p < 0.05$). Avulsion and bifurcation are shown to occur simultaneously based on the non-unimodal distribution of dimensionless island sizes created in our model, even though these are mechanistically different processes. Comparing our findings to natural deltas, we find consistent avulsion timescale-topset slope (T_a -S_{topset}) relationships. Our findings show how the delta topset slope serves as the first order control of the avulsion timescale, and how avulsion and bifurcation interact throughout delta building processes. This interaction is significant due to their direct impact on coastal and inland hazards that arise from rapid geomorphic change and flooding on densely populated deltas.

Plain Language Summary

River deltas grow by distributing sediments along their channel courses. When channels become blocked with sediment, they can abruptly change course, which can cause devastating floods to people, infrastructure and landscapes. The timing and the processes associated with this channel course "switching" are currently less known. Using a computer model, we create virtual river deltas to understand how their networks of channels develop and switch during delta growth over a 400-year period. We find that the steeper the delta plain, the faster this abrupt change of channel course occurs. We also find that whilst a river delta grows, channels may change course both close to the delta's shoreline and along the delta plain at the same time. Our model predictions of channel course timings are very consistent with those observed from natural river deltas. We now more fully understand the timing and the interactions of abrupt channel changes on deltas, a finding that could potentially reduce flood risk.

Introduction

River deltas are home for ~339 million people worldwide, are hotspots for biodiversity, and crucial carbon sinks (Ericson et al., 2006; Hackney et al., 2020; Loucks, 2019; Shields et al., 2017; Syvitski & Saito, 2007). However, the geomorphic dynamism of river deltas in the modern era has been altered by growing stressors such as change in hydrologic regimes, sea-level rise, and accelerated subsidence (Giosan et al., 2014; Syvitski et al., 2009; Tessler et al., 2015; Wallace et al., 2014), putting human and other systems that rely on river deltas at considerable risk. To anticipate how river deltas may respond to these growing pressures, we need to understand how deltas internally (i.e. autogenically) build and evolve through time.

River delta growth depends on upstream catchment properties as inputs of water and sediment, and also as the (external) cause of the gradient of the input river to the delta plain. The growth of a river delta is initiated through repeated mouth bar deposition due to sudden expansion and deceleration of a sediment-laden jet of water entering relatively still water, usually the sea or a

lake (Bates, 1953; Edmonds et al., 2011; Kleinhans et al., 2013; Wright, 1977). Mouth bars grow in both upstream and downstream directions from the point of initiation, reach a height of around 0.4-0.6 of the initial flow depth, and stop growing once the sediment flux is advected around the mouth bar rather than accelerated over the bar (Edmonds & Slingerland, 2007; Fagherazzi et al., 2015; Kleinhans et al., 2013). Simultaneously, avulsion takes place in more upstream parts of a delta plain when mouth-bar deposition and stagnation induce parent channel backfilling, triggering an avulsion to create a smaller channel by breaching the channel levee in the upstream part of a mouth bar (Ganti, Chadwick, Hassenruck-Gudipati, & Lamb, 2016). Another type of avulsion involves blocking of a channel by sediment advected from upstream, promoted by in channel aggradation that is independent from the distal process (Kleinhans et al., 2013). Overall, the combination of bifurcation and avulsion creates a distributary channel network that merges upstream at the delta apex (Edmonds & Slingerland, 2007).

Many studies have shown that different processes are involved in the mechanics of avulsion and bifurcation in river deltas (Chatanantavet et al., 2012; Edmonds et al., 2009; Edmonds & Slingerland, 2007; Ganti, Chadwick, Hassenruck-Gudipati, Fuller, et al., 2016; Jerolmack & Swenson, 2007; Kleinhans & Hardy, 2013). Based on different processes that dominate within each, a river delta may be divided into bedslope-mediated and backwater-mediated zones (Ganti et al., 2014; Prasojo et al., 2022). The bedslope-mediated zone consists of the river environment downstream as far as the first avulsion point, initiating the onset of delta building and avulsion-driven stratigraphy. In contrast, the backwater-mediated zone consists of delta distributary channels down to the delta shoreline, with backwater-triggered avulsion or bifurcation dominating the stratigraphy.

The bedslope-mediated zone is controlled by in-channel aggradation (Prasojo et al., 2022), demonstrated by the strong correlation between the upstream slope and the location of avulsion nodes based on the study of 105 natural deltas. In-channel aggradation can then trigger avulsion by incision (Slingerland & Smith, 2004), partial avulsion (Kleinhans et al., 2013) or full avulsion (Prasojo et al., 2022). In contrast, bifurcation in the backwater-mediated zone of a delta is caused by channel splitting around the mouth bar due to flow deceleration when entering a relatively still body of water (Edmonds & Slingerland, 2007; Ganti, Chadwick, Hassenruck-Gudipati, & Lamb, 2016; Olariu & Bhattacharya, 2006). This phenomenon can then induce channel backfilling that can also act as an avulsion trigger in the backwater-mediated zone. Hence, we may have bifurcation-triggered avulsion located within the backwater-mediated zone, as also found in Huanghe (Yellow) delta by Ganti et al. (2014).

However, our knowledge about the internal interdependency between avulsion and bifurcation is limited, despite their direct influence on coastal and inland flood risk on river deltas. Hypothetically, catchment properties have varying slope gradients located upstream of a deltas first avulsion point. These catchment properties control transport capacity and the sediment flux feeding into

a delta. Consequently, these top-down properties also play an important role in controlling the avulsion length of a delta. With homogeneous sediment size and constant input of water and sediment discharge, steeper upstream slopes will lead to larger deltas and more frequent avulsion and bifurcation. Conversely, lower upstream slopes lead to smaller river deltas and slower avulsion and bifurcation processes. If this hypothesis is true, upstream slope may exert an important role in defining the frequencies of both avulsion and bifurcation in river deltas. Since our understanding of the internal controls triggering avulsion-bifurcation response is currently underdeveloped (Ganti et al., 2014; Kleinhans et al., 2010), this investigation aims to: (1) identify the first order controls of avulsion and bifurcation timescales from a suite of numerical model experiments that have various upstream slopes; (2) understand the avulsion-bifurcation causalities through investigation of each step of the delta building process; and, (3) assess the implications from this numerical model for understanding the dynamics of contemporary and ancient deltas. Further, a robust understanding of these processes has practical implications due to their direct impact on coastal and inland flood risk on highly populated river deltas. We created a suite of numerical simulations with six different scenarios representing different upstream slopes, based on natural river deltas, to understand autogenically-controlled avulsion and bifurcation.

Methods

We designed a set of numerical experiments to model a natural scale river delta (7.5 x 7.5 km) where we control the slope upstream of the delta avulsion node (S_{US}) while keeping other physical parameters constant. We adopted the Delft3D river delta models from Edmonds & Slingerland (2010) and Caldwell & Edmonds (2014), with bathymetry modified as necessary to accommodate our various upstream slopes. The physical parameters set in the model were based on real deltas and we measured the avulsion timescale (T_a) based on the analytical approach by Chadwick et al. (2020) and the bifurcation timescale (T_b) using the scaling approach of Coleman & Wright (1971) .

Scenario

The model uses various slopes upstream of the slope break location (Fig. 1a), with slopes chosen to be representative of natural river deltas. The slopes upstream (S_{US}) and downstream (S_{DS}) of slope breaks identified from 105 globally distributed river deltas from Prasojo et al. (2022) were used to calculate the ratio of upstream:downstream slopes, from which we determine representative percentiles of this ratio (Fig. 1b; Table 1). These representative percentiles were then used to calculate upstream slope values in the model assuming constant initial downstream slope (S_{DS}=0.000375) from the Mississippi delta (Edmonds & Slingerland, 2010).

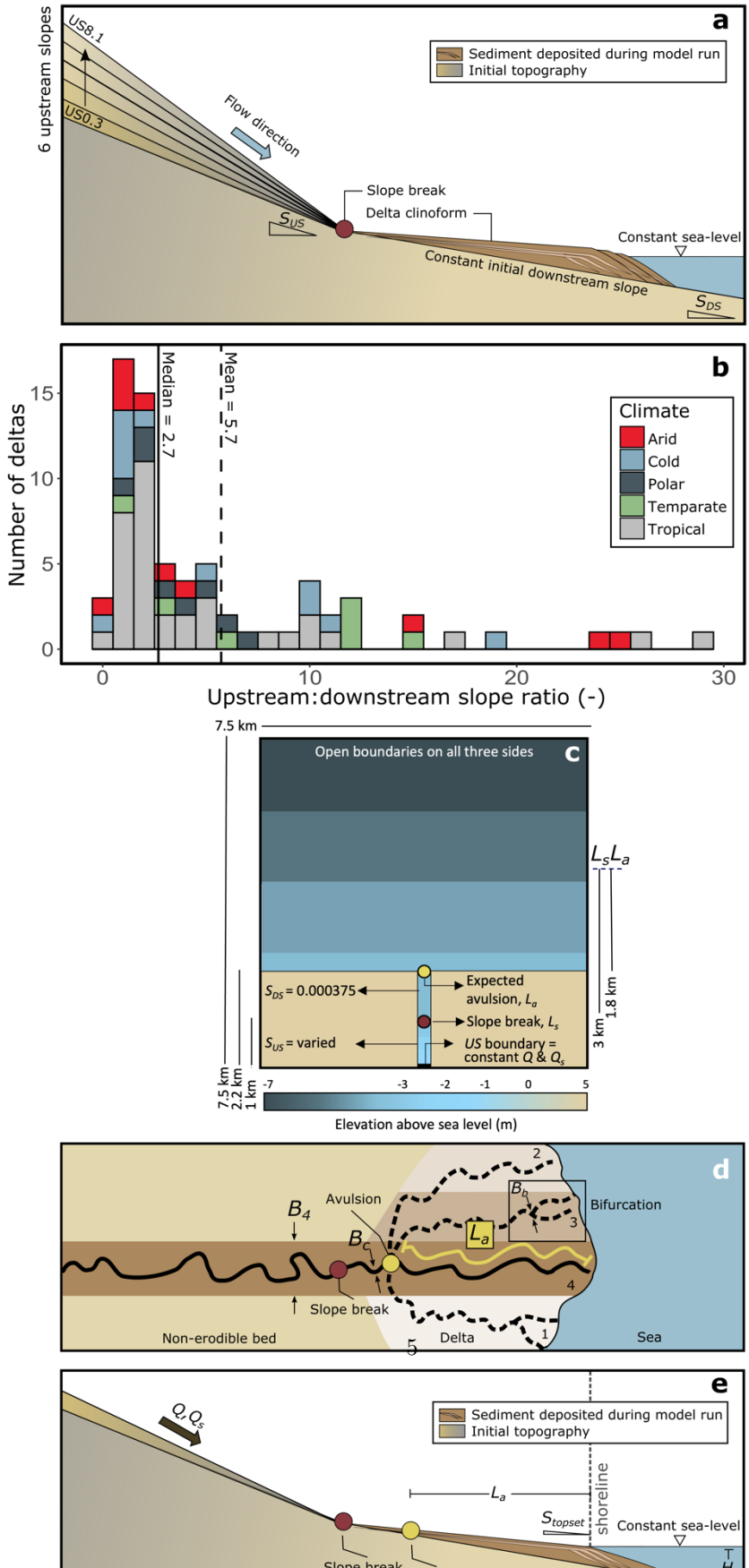
a
6 upstream slopes
US8.1
US0.3
Flow direction
Slope break
Delta clinoform
S_{US}
Constant sea-level
Constant initial downstream slope
S_{DS}
Sediment deposited during model run
Initial topography
b
Number of deltas
Median = 2.7
Mean = 5.7
Climate
Arid
Cold
Polar
Temparate
Tropical
Upstream:downstream slope ratio (-)
c
7.5 km
Open boundaries on all three sides
$L_s L_a$
S_{DS} = 0.000375
Expected avulsion, L_a
Slope break, L_s
S_{US} = varied
US boundary = constant Q & Q_s
3 km
1.8 km
7.5 km
2.2 km
1 km
Elevation above sea level (m)
d
B_4
Avulsion
B_c
B_b
Bifurcation
L_a
Slope break
Non-erodible bed
Delta
Sea
e
Q, Q_s
Sediment deposited during model run
Initial topography
L_a
shoreline
S_{topset}
Constant sea-level
Slope break

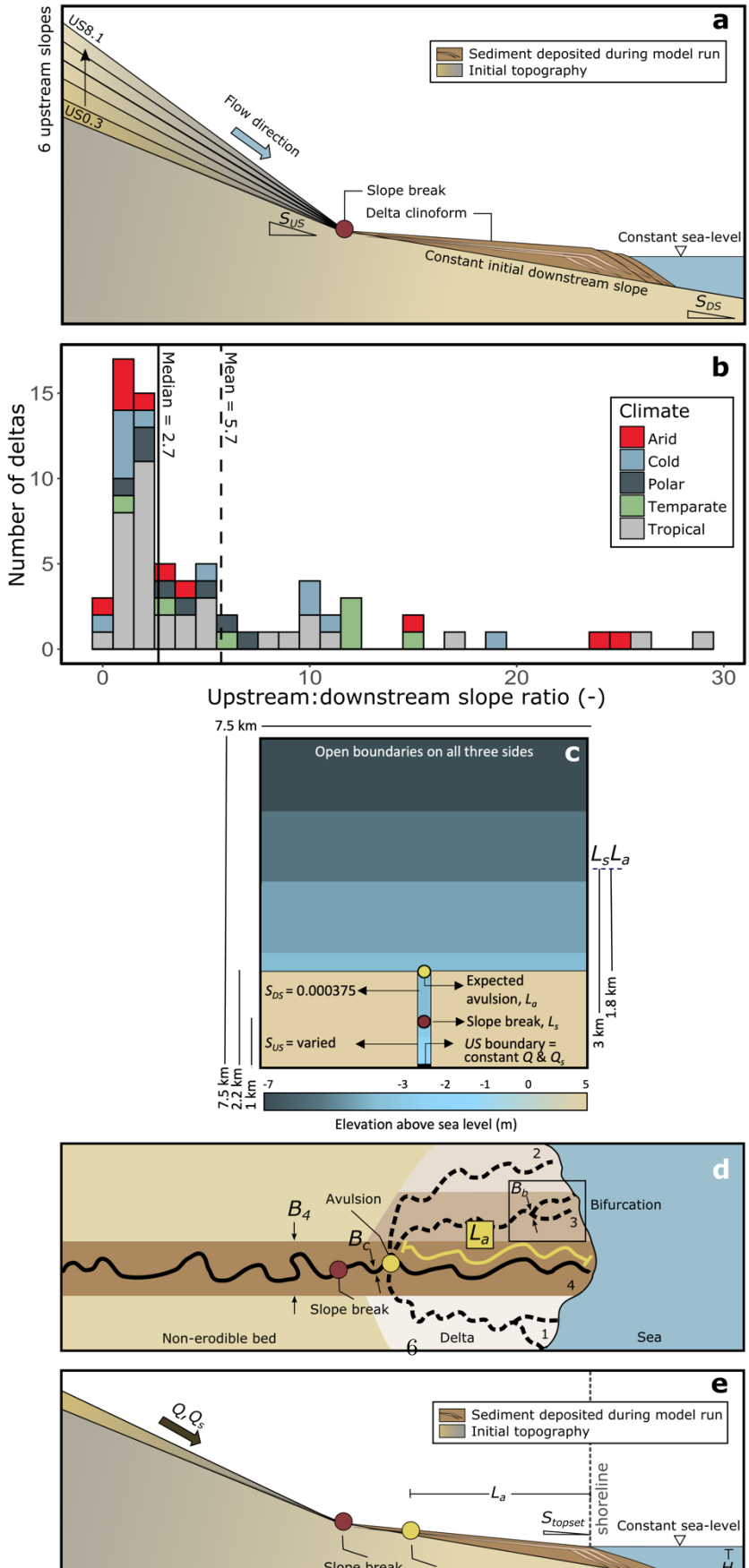
a
6 upstream slopes
US8.1
US0.3
Flow direction
Sediment deposited during model run
Initial topography
Slope break
Delta clinoform
S_{US}
Constant sea-level
Constant initial downstream slope
S_{DS}
b
Number of deltas
Median = 2.7
Mean = 5.7
Climate
Arid
Cold
Polar
Temparate
Tropical
Upstream:downstream slope ratio (-)
c
7.5 km
Open boundaries on all three sides
$L_s L_a$
S_{DS} = 0.000375
Expected avulsion, L_a
Slope break, L_s
S_{US} = varied
US boundary = constant Q & Q_s
3 km
1.8 km
7.5 km
2.2 km
1 km
Elevation above sea level (m)
d
B_4
Avulsion
B_b
Bifurcation
B_c
L_a
Slope break
Non-erodible bed
Delta
Sea
e
Q, Q_s
Sediment deposited during model run
Initial topography
L_a
shoreline
S_{topset}
Constant sea-level
Slope break

Table 1. Numerical modelling scenarios. IDs refer to ratio of the upstream slope (US) to the downstream (L

Run ID
US0.3
US0.68
US1.4
US2.7
US6
US8.1

Model setup

We use Delft3D (4.04.02) software (Deltares, https://oss.deltares.nl/web/delft3d) to model six different scenarios. Delft3D is a physics-based model that simulates the hydrodynamics and morphodynamics of environments including rivers, estuaries and river deltas (Edmonds & Slingerland, 2010; Caldwell & Edmonds, 2014; Nienhuis et al., 2018a;b). The software has been validated for a wide range of environments, including self-formed river deltas (Edmonds & Slingerland, 2007, 2008; Geleynse et al., 2011; Morgan et al., 2020; Nienhuis, Törnqvist, et al., 2018; Nijhuis et al., 2015; Rossi et al., 2016; Williams et al., 2016). Flow is computed using the depth-averaged, nonlinear, shallow-water equations, obtained from three-dimensional Reynolds-averaged Navier-Stokes equations (Edmonds & Slingerland, 2010). The velocity distribution in the model is then used to compute sediment transport (only suspended load is applied in our model) and to update the bed elevation (or bathymetry) according to divergence in sediment transport (Caldwell & Edmonds, 2014).

We adopted the geometry and physical parameters from a synthetic self-formed river delta model ('scenario o') from Edmonds & Slingerland (2010) and Caldwell & Edmonds (2014) (Fig. 1c). The model is rectangular with four boundaries, the incoming river discharge being located at the 'South' boundary of the model and the other three boundaries set to 0 m elevation above sea level. The incoming river discharge, uniformly spreads across the 250 m wide inlet channel, is constant at 1050 m^3/s, a representative value for global river discharge (Caldwell & Edmonds, 2014; Edmonds & Slingerland, 2010), and sediment discharge was in equilibrium with transport capacity at this inlet. The model was enlarged to 7.5 km x 7.5 km to avoid the delta plain extending across the model boundaries. We modified the upstream part of the model domain by introducing a slope break and slope-avulsion length scaling (L_a:L_s = 6:10) that we determined from modern systems (Fig. 1c, Table 1) to accommodate different upstream slope scenarios. Modification of the upstream part of the model domain involves changing the bathymetry to introduce this slope break - avulsion length scaling. We maintained other physical (e.g. grain sizes, critical bed shear stress for erosion and deposition) and numerical parameters constant across all scenarios (Table 2). Moreover, we ran additional sensitivity analyses using 25 subsurface layers instead of one to see its impact on the stratigraphy produced

in each scenario.

Table 2. User-defined model parameters (adopted from Edmonds & Slingerland (2010); Caldwell & Edmond

Parameter
Grid size
Cell size
Run duration
Downstream basin bed slope
Initial channel dimension (width x depth)
Upstream non-erodible bed elevation
Initial upstream length
Initial avulsion length from the expected shoreline
Initial slope break length from the expected shoreline
Inlet open boundary: water discharge
Downstream open boundary: constant water surface elevation
Initial sediment layer thickness at bed
Number of subsurface stratigraphy bed layers
Time step
Morphological scale factor
Spin-up interval

Surface metrics

We define avulsion and bifurcation timescales as the times needed for the delta distributary channel to create one avulsion or bifurcation, respectively. The analytical model for calculating avulsion timescales assumes switching of flow and sediment partitioning between multiple lobes in a delta plain, and considers the influence of backwater hydrodynamics in calculating the avulsion timescale (Chadwick et al., 2020).

Chadwick et al. (2020) derived the avulsion frequency as:

$$f_a = \frac{1}{(1-\lambda_p)} \frac{Q_s}{(L_a - D)BH + DB\left(H_b + z + \frac{DS_{\text{topset}}}{2}\right)} \; if \; D \geq 0 \quad (1)$$

$$f_a = \frac{1}{(1-\lambda_p)} \frac{Q_s}{L_a \text{BH}} \; if \; D < 0 \quad (2)$$

$$D = (H - z)/S_{\text{topset}} \quad (3)$$

$$H = H^* h_c \quad (4)$$

with the bankfull depth calculated using Parker et al.'s (2007) method:

$$h_c = \left(\frac{C_f {Q_c}^2}{g {B_c}^2 S_{\text{topset}}}\right)^{\frac{1}{3}} \quad (5)$$

with f_a = avulsion frequency [year], Q_s = sediment load [km^3/year], B = lobe width of each avulsion [km], L_a = avulsion length [km], $_p$ = sediment porosity [-], H = aggradation thickness necessary for avulsion [m], H_b = basin depth [m], H^* = avulsion threshold [-] = 0.2-1.4 in lowland deltas (Ganti et al., 2019), h_c = bankfull depth [m], C_f = bed friction coefficient [-], Q_c = bankfull discharge [m^3/s], B_c = channel width at avulsion node [m], S_{topset} = topset slope [-], D = lobe-progradation distance [km] and z = magnitude of sea level rise [m].

We assume the avulsion threshold (H^*) to be 0.5, which is realistic for lowland deltas (Ganti et al., 2019), and $D > 0$ since there is no allogenic forcing that would make the delta regress. Since sea-level is constant in this investigation, sea level rise $z = 0$. Sediment porosity ($_p$) is assumed to be 0.4 (Jerolmack, 2009), bed friction coefficient (C_f) = 0.002 for lowland rivers (Parker et al., 2007), and bankfull discharge (Q_c) = 1050 m^3/s. The upstream sediment boundary condition is for the inlet to be in equilibrium so that sediment load changes every timestep to match the sediment transport capacity at the inlet. We use equation (1) to calculate avulsion timescale (T_a = 1/avulsion frequency) throughout the model run.

To calculate the bifurcation timescale, we adopted the approach of Coleman & Wright (1971) (also used by Swenson (2005) and Jerolmack & Swenson (2007)). Coleman & Wright (1971) discovered that the length of distributary channels (L_D) in between adjacent bifurcation nodes in a delta plain scales with the channel width upstream of the bifurcation (B_b) (L_D 10 B_b). For a river delta without any wave or tide influence, delta progradation rate (v_p) can be written as:

$$v_p = \frac{Q_s}{B_b H_b} \quad (6).$$

Consequently, the bifurcation timescale is

$$T_b = \frac{L_D}{v_p} = \frac{\alpha B_b}{Q_s}.B_b H_b = \frac{\alpha {B_b}^2 H_b}{Q_s} \quad (7)$$

with = dimensionless parameter 10 (Coleman & Wright, 1971), Q_s = sediment load (km^3/year), and H_b = basin depth (m) (Jerolmack & Swenson, 2007; Swenson, 2005). The basin depth (H_b) is kept constant at 7.5 m since we do not introduce sea-level rise in any scenario (Edmonds & Slingerland, 2010).

All the surface metrics are measured once the model has reached a dynamic equilibrium state in which the sediment load (Q_s) that a channel must transport is balanced by the water discharge (Q) supplied to the channel and the channel slope (S) (Lane, 1954). The lobe width of each avulsion (B), channel width at avulsion nodes (B_c), channel width upstream of a bifurcation (B_b) and avulsion

length (L_a) were measured in QGIS from the georeferenced images produced by Delft3D at every timestep. Topset slope (S_{topset}) for every timestep was measured from a longitudinal cross-section located through the centre of the model by conducting linear regression through topset elevation points. Lobe progradation distance (D) and bankfull depth (h_c) were calculated using Eq. 3 and 5 consecutively to obtain the avulsion timescale at each timestep during delta building. The model produces 52 computational timesteps in total, which equals ~400 years.

The calculated avulsion and bifurcation timescales are related to the measured topset slopes (S_{topset}) to assess the role of topset slope in affecting avulsion and bifurcation mechanisms. We recorded the stratigraphy produced during each run using representative transverse (E-W) and longitudinal (S-N) cross sections at every timestep. Transverse profiles are located at: proximal (2.38 km downstream of the model South boundary); medial (4.5 km); and distal (5.25 km) locations on the delta plain. The model results are then compared to avulsion and bifurcation timescales obtained from 19 modern river deltas, two fan deltas and one physical model that cover similar topset slope magnitudes to our model. Avulsion timescales from the natural and physical deltas are calculated using Eq. 1, with the dataset available from Chadwick et al. (2020) (Table S1). Bifurcation timescale is calculated using Eq. 7, using Q_s from Chadwick et al. (2020) and assuming the channel width at avulsion nodes (B_c) the channel width upstream of a bifurcation (B_b). Finally, we discuss our model's implications for natural systems by drawing on Jerolmack & Mohrig's (2007) and Chadwick et al's (2020) results.

Results

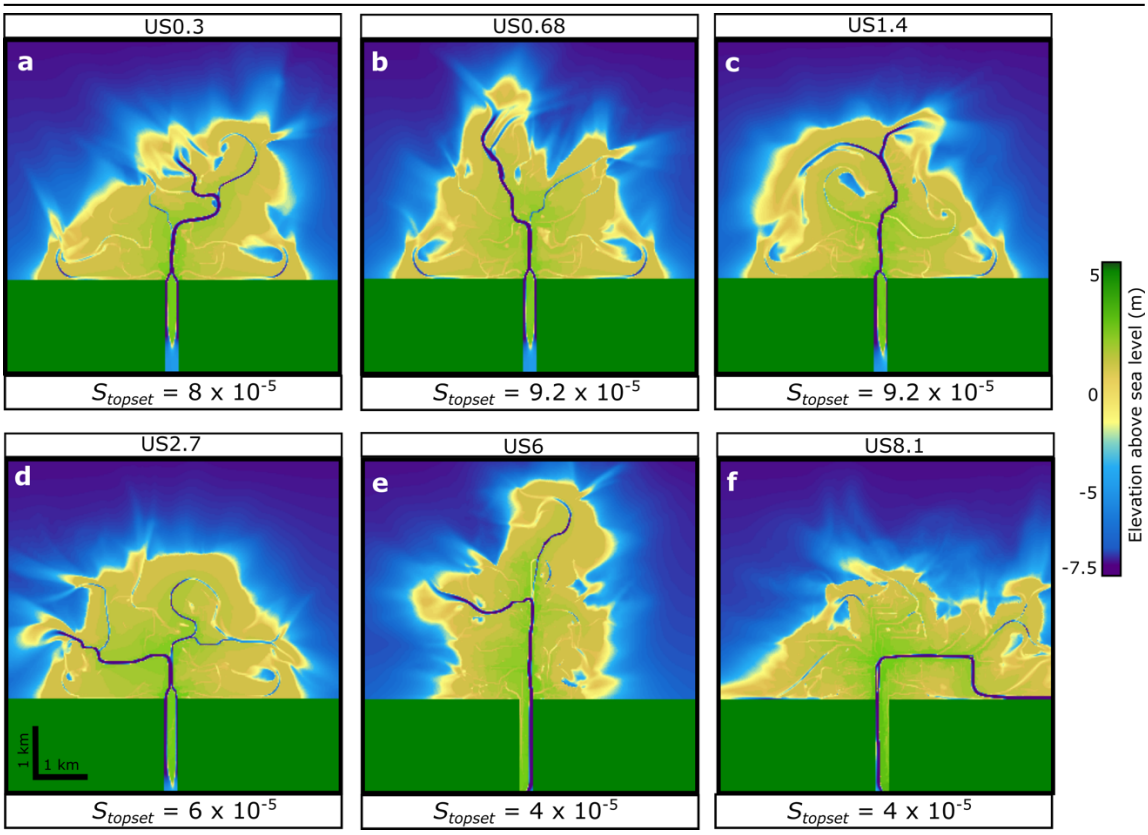

Figure 2. (a-f) Terrain models at the final time step of each scenario.

Delta plain morphology

Fig. 2 shows the morphology of the deltas in each scenario at the final timestep. Overall, the different upstream slopes produce variable topset slopes, and the resulting delta plains show different shoreline configurations, different numbers of active distributary channels and slightly different delta plain sizes. One delta plain reached the model boundary (US8.1) and this scenario was repeated with a larger domain size (see Supporting Information Fig. S1) and the avulsion and bifurcation timescales were calculated from this larger domain.

Steeper upstream slopes are associated with longer avulsion lengths (L_a) (Fig. S2a) and larger lobe widths created by each avulsion (B) (Fig. S2b). However, steeper upstream slopes produce slightly narrower channel widths upstream of a bifurcation (B_b) (Fig. S2c) with no impact on the channel width at the avulsion node (B_c) (Fig. S2d). Statistical significance tests (one-way ANOVA and Kruskal-Wallis tests applied to normally- and non-normally distributed data, respectively) show that upstream slopes significantly control the geometry

variables of the river deltas measured in this study ($p < 0.05$).

Figure 3 shows the distribution of avulsion and bifurcation timescales, noting that these can be examined at different times during each run. The range of avulsion and bifurcation timescales span different orders of magnitude from both between-scenario and within-scenario variability. Avulsion period ranges from 1.2 x 10^3 - 1.9 x 10^5 year (median = 1.2 x 10^4 year; N = 229) (Fig. 3a). Bifurcation timescales are in the range of 2 x 10^{-2} - 5.7 years (median = 4 x 10^{-1} year; N = 201) (Fig. 3b; Fig. S3). The different magnitudes in response times for avulsion and bifurcation processes may be caused by the different compensation scale, the tendency for sediment to preferentially fill lower topography, and also by different channel depths and aggradation rates between the upstream (i.e. bedslope-mediated) and downstream (i.e. backwater-mediated) parts of deltas (Jerolmack & Paola, 2010; Li et al., 2016, 2018; Straub et al., 2020).

Across all the scenarios, the distributions of the avulsion and bifurcation timescales remain constant (Fig. 3a,b). One-way ANOVA shows that the scenario (upstream slope) does not significantly influence ($p > 0.05$) the avulsion timescale. However, there is a significant influence of the upstream slope on the bifurcation timescale (ANOVA; $p < 0.05$). Correlations between the other independent variables (B, B_c, and L_a) and the avulsion and bifurcation timescales (Fig. S4) are generally not significant, although some do have significant (e.g. T_a-B, T_a-L_a), although weaker than the avulsion timescale-topset slope (Fig. 3c), correlations.

To understand the first order control of these avulsion and bifurcation timescales, we examine the independent variables used in their calculation. The topset slopes (S_{topset}) play a significant role in defining the avulsion timescale (Fig. 3c) but not in the bifurcation timescale (Fig. 3d). The avulsion timescale (T_a) has a statistically significant negative power law relationship with the topset slope ($T_a = 0.3{S_{topset}}^{-1.18}$; $R^2 = 69\%$, $p < 0.05$) (Fig. 3c).

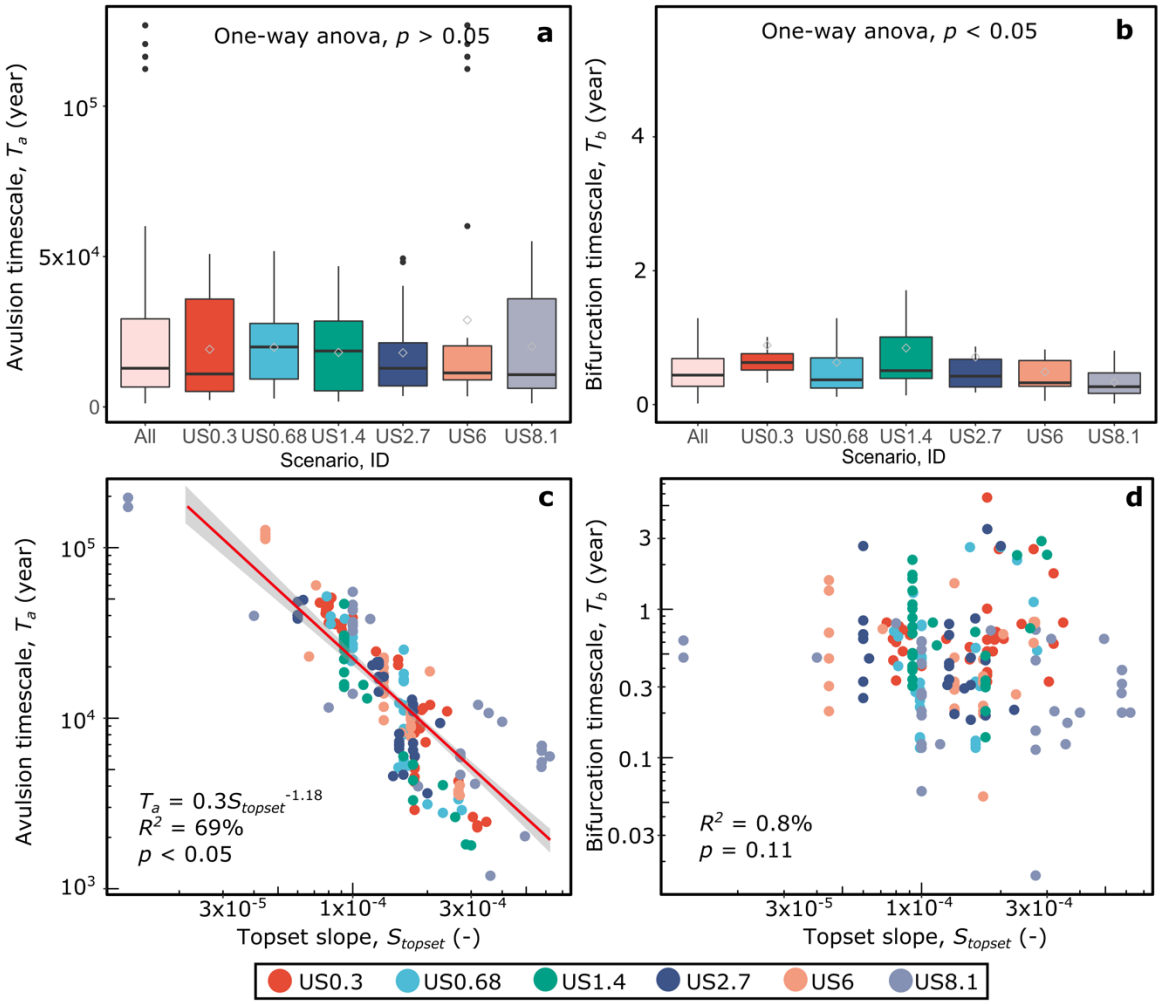

Figure 3. (a-b) Distributions of avulsion and bifurcation timescales for all model and individual scenarios. (c

Stratigraphy during delta growth

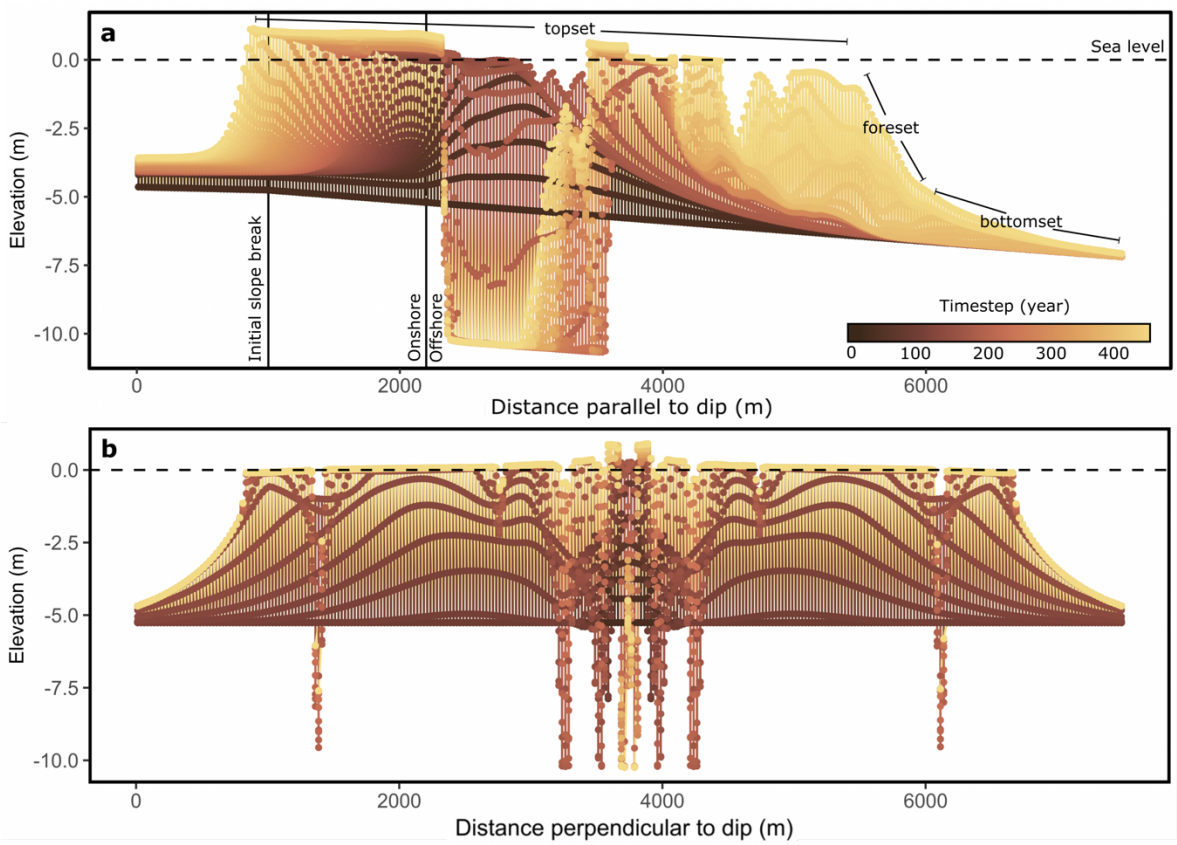

Figure 4. (a). Longitudinal cross section (S-N on Figure 1) showing the stratigraphy produced for each time

Fig. 4a shows the evolution of the delta including both foreset progradation and topset aggradation. These elevation data enable examination of changes to bathymetry during each timestep. Sedimentation occurs simultaneously offshore and within the input channel within the valley at the head of the delta. The transverse proximal cross section shows that distributary channels reach similar depths across all timesteps (Fig. 4b). Note that the deep channel erosion located at 2.2 - 3.6 km on Fig. 4a is caused by a full depth erosion mixing of a five-metre-thick subsurface layer. Sensitivity analyses using 25 subsurface layers produced similar topography (Fig. S5).

The elevations from transverse cross-sections of the delta plain at representative proximal, medial and distal sections are summarised as boxplots (Fig. 5). The elevations are consistent in all cases, although US6 has slightly higher topography due to a longer and straight distributary channel developing (Fig. 2e). Overall, the down-dip longitudinal section and the transverse cross sections all produced elevations that are statistically similar across all scenarios and all

timesteps (Table 3).

Table 3. Summary elevations from topographic profiles at all timesteps in all model scenarios. Data from longitudinal (S-N on Figure 1) and transverse (proximal, medial and distal) cross sections are shown. SL = sea-level.

	Longitudinal	Transverse[1]						
			Proximal	Medial	Distal			
	Above SL	Below SL	Above SL	Below SL	Above SL	Below SL	Above SL	Below S
Max	1.30	11.45	1.35	10.25	0.81	11.05	0.62	11.31
Mean	0.35	5.65	0.17	3.64	0.13	4.93	0.11	5.47
Median	0.33	6.18	0.09	4.57	0.10	5.53	0.05	5.99
Min	0.00	0.00	0.00	0.00	0.00	0.00	0.00	0.00
N	10346	98802	42097	108703	5463	145337	879	149921

[1]Transverse profiles located at: proximal node 95 (2.38 km downstream of the model boundary); medial node 180 (4.5 km); distal node 210 (5.25 km).

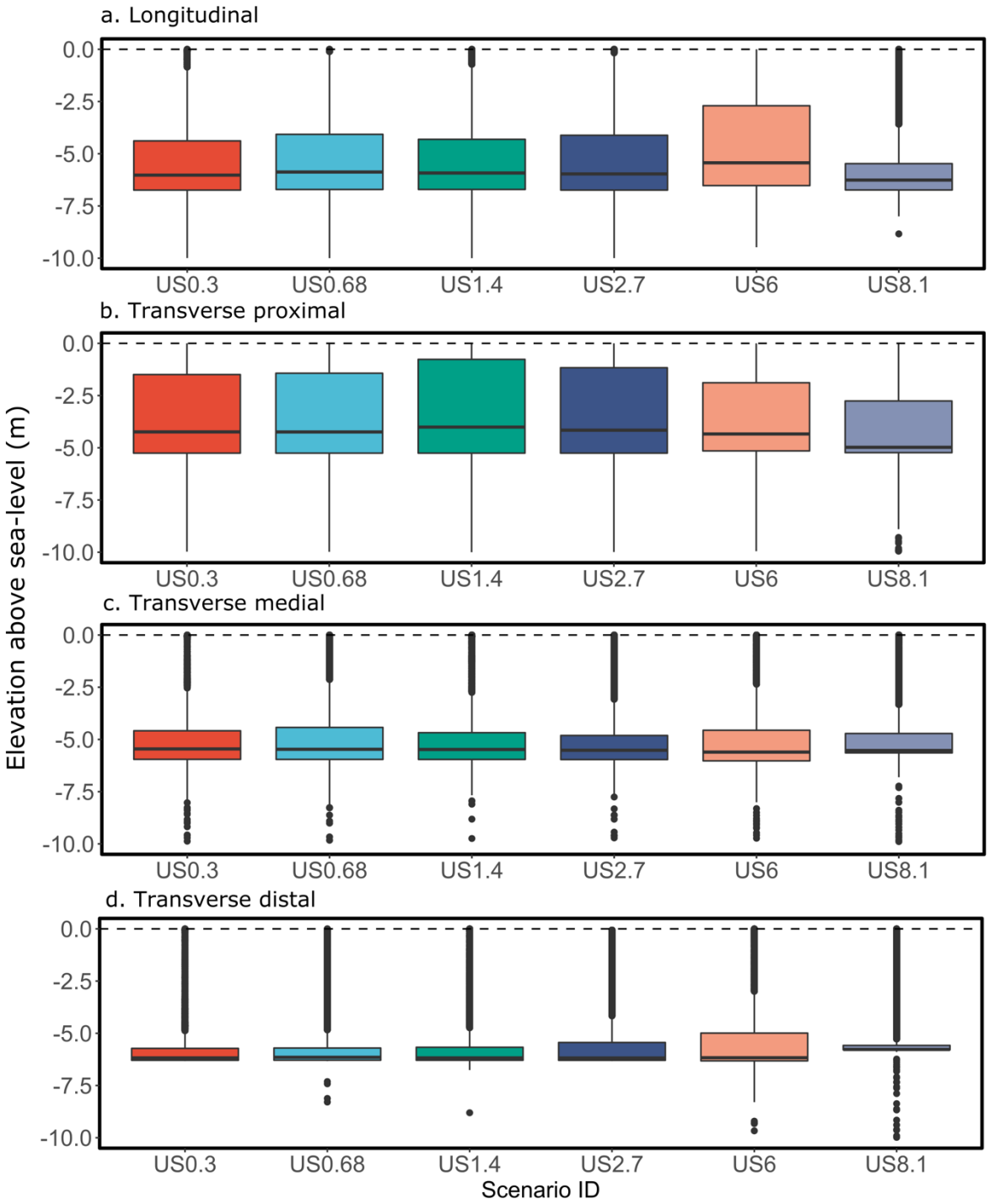

Figure 5. Boxplots of topographic elevation for each scenario from: (a) longitudinal cross section; (b) proxim

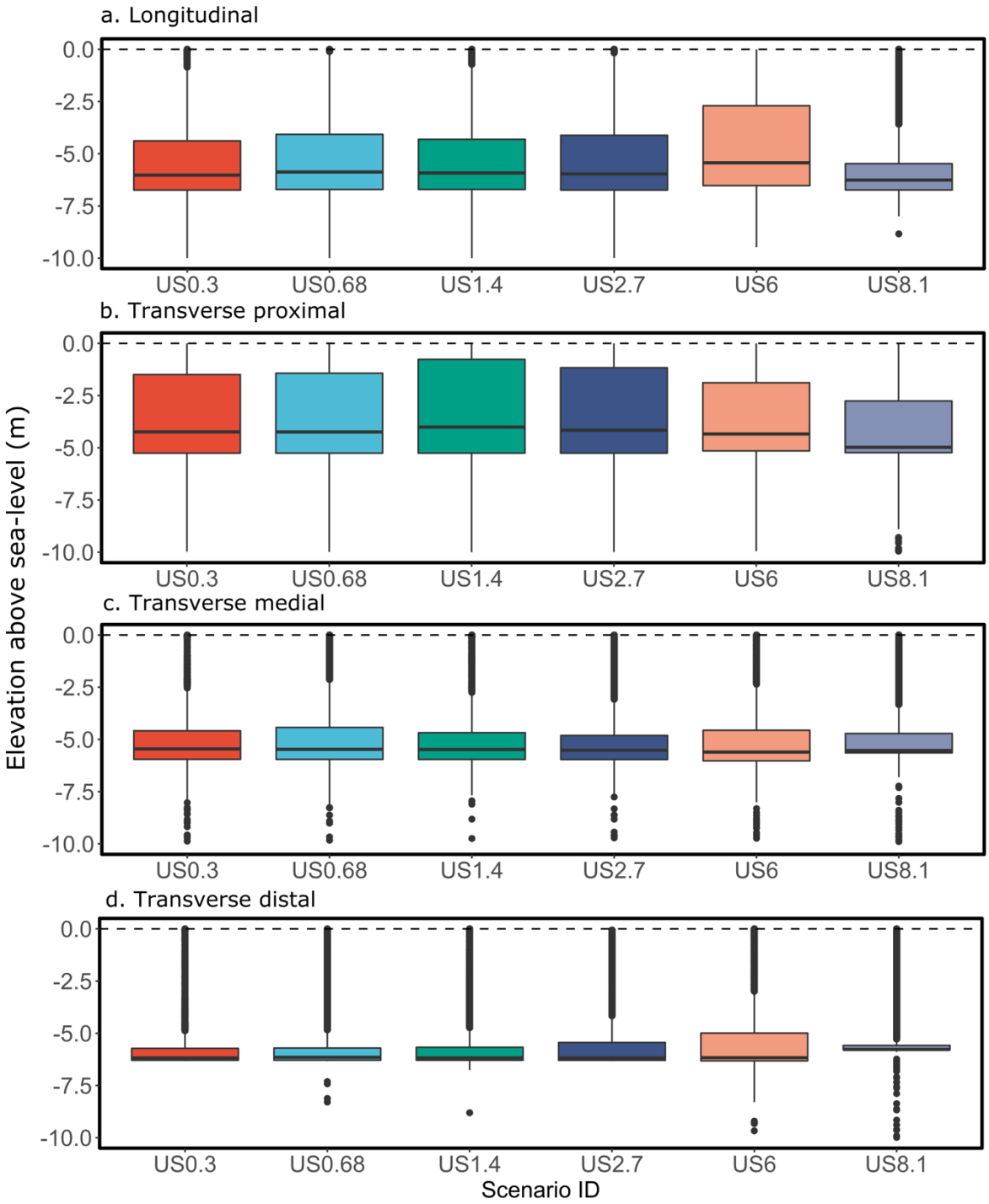
a. Longitudinal
b. Transverse proximal
c. Transverse medial
d. Transverse distal
Elevation above sea-level (m)
0.0
-2.5
-5.0
-7.5
-10.0
US0.3
US0.68
US1.4
US2.7
US6
US8.1
Scenario ID

Discussion

The six scenarios used in this study provide details of avulsion and bifurcation processes from the inception of delta building. Since avulsion is infrequent, by calculating the avulsion and bifurcation timescales of each timestep we can estimate the range of possible magnitudes of these processes (assuming that the equations we used are accurate). Correlation with the independent parameters that we control during the modelling suggests that topset slope provides the first order control of avulsion timescales. The avulsion-bifurcation causalities and their implications for the contemporary and ancient deltas are also discussed in the following sections.

First-order control of avulsion and bifurcation timescales

The avulsion timescale is strongly correlated with the topset slope at each timestep (Fig. 3c). The topset slope is partly a function of the scenario (which determines upstream slope). However, when being compared across scenarios, none of the scenarios show a strong correlation with the avulsion timescale (Fig. 3a) and the topset slope produced. Correlations between avulsion and bifurcation timescales and other independent variables (Fig. S4) also show weak to no correlations. Moreover, correlating the bifurcation timescale to the width upstream of a bifurcation (B_b), the only varied independent variable in this experiment, shows exponential relationship as expected from the Eq. 7.

The independent variables that we correlate with the avulsion and bifurcation timescales are all geometrical (avulsion length, lobe size, channel widths). Importantly, none of these variables are well-correlated with the avulsion or bifurcation timescales. These results imply that avulsion and bifurcation timescales may not be dependent on the geometry of the delta or the size of the delta. Rather, topset slope may be the variable that controls the avulsion timescale (Fig. 3c). The topset slope controls the avulsion timescale due to stream power increasing with steeper topsets and hence avulsion occurs more frequent in a steeper delta plain. The topset slope itself is mainly controlled by the top-down forcing of in-channel vertical aggradation. While the bifurcation timescale is controlled by the width upstream of a bifurcation (B_b) as shown in the Eq. 7 and directly related to the sediment load (Q_s), which we do not vary in this study. Significant correlation between scenario and bifurcation timescale shown in Fig. 3b may be caused by statistical artefacts. Further statistical analysis shows that bifurcation timescale does not correlate with the upstream slopes used to define the scenarios, with $R^2 = 7.6\%$.

In river deltas, fine-grain and cohesive sediment frequently dominate the system since sediment loads fine downstream. With finer and more cohesive sediments and possibly more vegetation, channel bars are stifled, promoting overbank floodplain deposition (Ielpi & Lapôtre, 2019; Kleinhans et al., 2018). With sinuous delta distributary channels and more stable riverbanks due to cohesive sediments, vertical aggradation is a more important geomorphic mechanism

than the lateral migration of distributary channels. Because of this, avulsion in river deltas is more likely to be progradational, in which the avulsion disturbs the surrounding delta plain rather than reoccupying pre-existing channels, in contrast to braided rivers (Supplementary Movie 1). This avulsion style is similar to the avulsion style of a meandering river investigated by Valenza et al. (2020); slope also serves as the important control of the avulsion in this channel type. In this avulsion style, top-down forcing of in-channel vertical aggradation, in which topset slope is its direct product, controls the likelihood for superelevated channel to discharge or avulse most of its water and sediment on to the surrounding water in the form of mouth bar deposition.

Although the topset slope controls avulsion timescale in this model, other potentially significant variables are held constant in our model (e.g. dz/dt, H_b, $_{p,}$ Q_s). Hence, further sensitivity studies on the effects of varying these other independent variables could be undertaken. As an example, since we set Q_s as a constant, we are excluding the influence of changes in Q_s on avulsion and bifurcation timescales that directly impacts in-channel aggradation rates and the avulsion or bifurcation thresholds (H or H^*). Chadwick et al. (2020) considered the influence of sea-level rise on the avulsion timescale. By integrating theory, numerical model and field datasets, they found that avulsion timescale is controlled by the balance between relative sea-level rise (z) and sediment supply (Q_s), where sea-level rise promotes a more frequent avulsion.

Stratigraphically, as shown in the consistency between delta size and shape and the proximal, medial, distal and parallel cross sections, changing the upstream slope in our scenario did not greatly influence the deposit thickness (Fig. 4a-d). This result is similar to the homogeneous thicknesses of stratigraphy from the Mississippi delta (Chamberlain et al., 2018). Comparing scenarios with a steeper slope (US6) with a gentler slope (US0.3) does not show deeper erosion (i.e. deeper autogenic reworking depth) or a thicker autogenic signal (i.e. thicker sediment deposited on foresets and topsets) (Fig. S5). The statistics in Table 3 corroborate that all the upstream slope scenarios maintain the autogenic signal and autogenic reworking depth in the model. Further statistical significance tests also show that topset slope significantly controls the avulsion length (L_a) and channel width at the avulsion node (B_c) but not the lobe width of each avulsion (B) or the channel width at bifurcation (B_b). Consequently, we hypothesize that the upstream slope may not control the magnitude of autogenic signals and hence that the topset slope only partly controls this magnitude.

We show in this study that neither the autogenic thickness nor the autogenic reworking depth (Ganti et al., 2020) are controlled by the upstream slope, shown by the similar topographic patterns in Fig. 4a-d and Table 3. The different upstream slopes may not influence the autogenic reworking depths due to the equilibrium sediment load and constant water discharge defined at the inlet boundary of the model. Autogenic reworking depths may be controlled either by sediment load and water discharge variability (Jerolmack & Paola, 2010; Li et al., 2016; Simpson & Castelltort, 2012) or by a non-equilibrium flow (Leary

& Ganti, 2020). Leary & Ganti (2020) found that the preservation of cross strata (i.e. autogenic signal) is higher under unsteady or non-equilibrium flow than under the equilibrium flow conditions used in this study. Consequently, varying discharge and/or sediment loads in further modelling work will provide a framework to assess how autogenic parameters could control the magnitude and/or timescale of avulsion.

The independence of the timescale and the magnitude of autogenic signals in our study may be influenced by the dynamic equilibrium upstream boundary condition. In the equilibrium state, the model keeps adjusting its sediment load (Q_s) to match its transport capacity in the prior timestep. We show that upstream slopes across an order of magnitude (Table 1) do not significantly influence the sediment load carried by the channel once the model has reached dynamic equilibrium. Consequently, similar volumes of sediment are being input to the delta across all scenarios, as shown by the relatively similar delta plain sizes (Fig. 2a-f). Although different upstream slopes may produce significantly different morphologies (avulsion length, delta lobe size, channel width at avulsion node and bifurcation node (Fig. S2)), the geomorphology of the delta plains does not significantly affect the bifurcation timescale, except that the avulsion timescale is determined by the topset slope (Fig. S4; Fig. 3c).

Avulsion and bifurcation causalities

In this section, we investigate the causalities between the avulsion and bifurcation processes in river deltas to assess whether bifurcation leads to avulsion through backward sedimentation processes (Ganti, Chadwick, Hassenruck-Gudipati, & Lamb, 2016; Hoyal & Sheets, 2009; Kleinhans, 2010; Reitz & Jerolmack, 2012), or vice versa. Visual observation of the model runs showed that avulsion and bifurcation may occur within the same timestep (Supplementary Movie 1). Jerolmack & Swenson (2007) hypothesized that bifurcation processes will dominate early in a delta's development. As bifurcation continues, a landward-shift in aggradation or channel backward sedimentation will trigger avulsion by in-channel deposition in more upstream reaches (Edmonds et al., 2009; Slingerland & Smith, 2004). Consequently, more established (or larger) deltas will be more avulsion-dominated or bedslope-mediated rather than bifurcation-dominated. Through time, the change in surface water slope induces a decrease in sediment transport capacity, triggering bedslope-mediated avulsion, particularly in proximal reaches, in more established or larger deltas (Ganti, Chadwick, Hassenruck-Gudipati, & Lamb, 2016).

Edmonds et al. (2011) modelled a theoretical delta by parameterising their model to enable bifurcation processes but prevent avulsion. When the island areas normalised by the total delta plain areas were measured, this theoretical delta has a unimodal distribution of normalised island area, as also found in the recent delta numerical models (Hariharan et al., 2021). Through time, a relatively older delta will deviate from this unimodality due to avulsion triggered by in-channel aggradation (Jerolmack & Swenson, 2007; Mohrig et al., 2000;

Slingerland & Smith, 2004) or due to the exposure of bedrock on the delta plain, as found in The Mossy delta (Edmonds et al., 2011).

By measuring the island size in all model runs, we produced distributions of normalised island area at each timestep (Fig. 6). There is no unimodality of the normalised island areas at any timestep in any of the model runs, which corroborates the interpretation of our data that bifurcation and avulsion occur simultaneously throughout the delta building process, as also suggested by model stratigraphy for all scenarios. Bifurcation never dominates the early delta building process, nor does avulsion dominate the later stage of the delta building process with both avulsion and bifurcation occurring throughout each simulation.

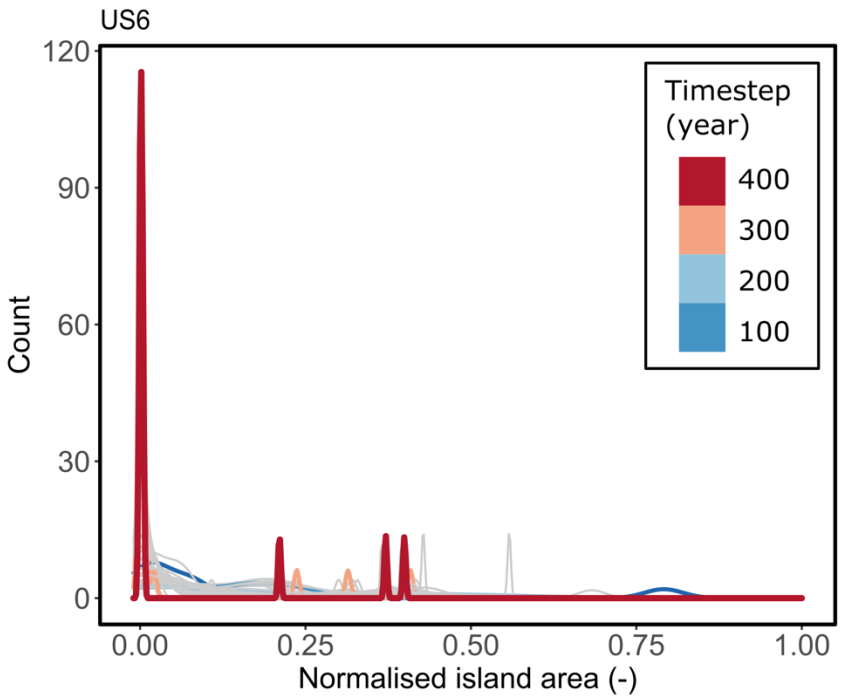

Figure 6. Distribution of normalised island area measured from US6 scenario showing multi-modality across

Implication for natural deltas

Data from natural deltas show a similar avulsion timescale-topset slope relationship to our model results, even though the natural and laboratory delta avulsion timescales are 1.5 orders of magnitude lower than in our models (Fig. 7a). Similarly, the relationships between bifurcation timescale to topset slope in natural deltas shows no correlation, consistent with our model results (Fig. 7b).

The lower order of magnitude of avulsion timescales in natural and laboratory deltas may be caused by allogenic forcings that we did not incorporate in our model. Sea-level rise rate, subsidence, variable sediment load, channel engineering and human-made avulsion can directly influence the avulsion timescales found in modern deltas (Heyvaert & Walstra, 2016; Pierik et al., 2018). Even though we show that there is no correlation between T_a-S_{topset} and the sea-level rise rate (dz/dt) as shown on Fig. 7, sea-level rise rate does play an important role in affecting the avulsion timescale in other studies (Chadwick et al., 2022; Li et al., 2022). Consequently, our models could imply that anthropogenic and allogenic forcing may reduce avulsion timescales, increasing the risk of avulsion for populations living on delta plains.

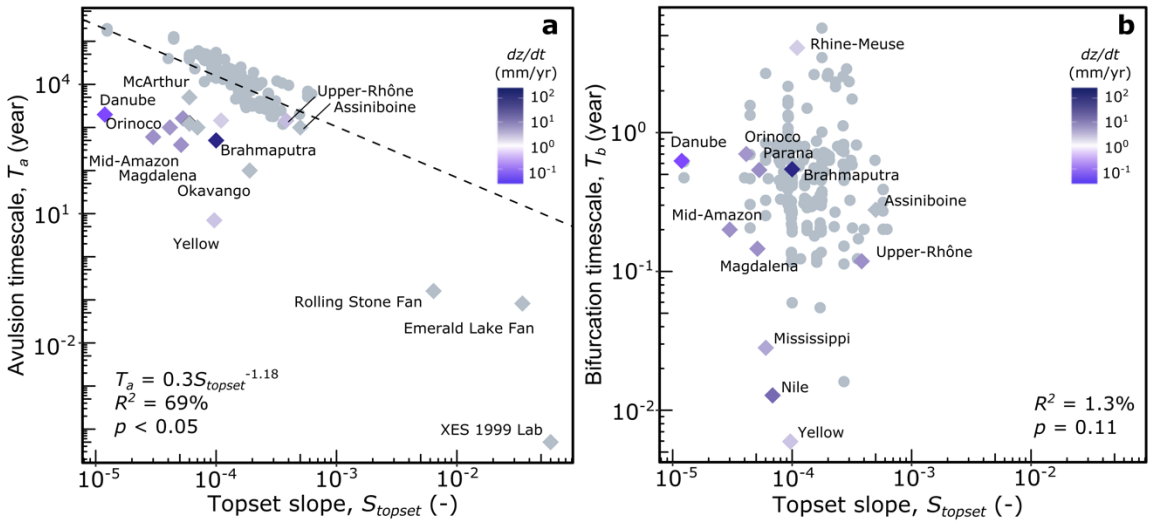

Figure 7. Relationships between: (a) avulsion timescale and topset slope; and (b) bifurcation timescale and

The avulsion timescales in our model span 10^1-10^5 years, whereas previous studies reported timescales of 10^1-10^3 years (Ganti et al., 2020). These avulsion timescales are sufficiently long that they overlap with the timescales of, and responses to, allogenic forcings that contribute to avulsion (e.g. base-level change) (Fig. 8). Hence, separating autogenic signals based on their timescales may not be effective due to the major overlap between these timescales. Consequently, a more careful examination of the preservation of allogenic base-level signal to the preserved stratigraphy is needed due to this long overlap. As an example, early investigation of spatial and temporal thresholds as the balance of input allogenic signal versus the system's autogenic signal suggest that a relatively smaller delta, in which the compensation time scale is smaller, will be more likely to preserve base-level change signal (Jerolmack & Paola, 2010; Li et al., 2016). Conversely, a relatively larger delta will be more likely to smear the

base-level change signal. However, in this study, we show that the autogenic timescale does not depend on delta geometry or sizes (Fig. S4). We imply that defining one dimensional temporal or spatial threshold is more complex than previously suggested (Toby et al., 2019, 2022). We suggest that disentangling autogenic and allogenic forcing in the rock record may need a more comprehensive perspective, adding data on sedimentary structures, fossil assemblages and other sedimentary features to morphological information.

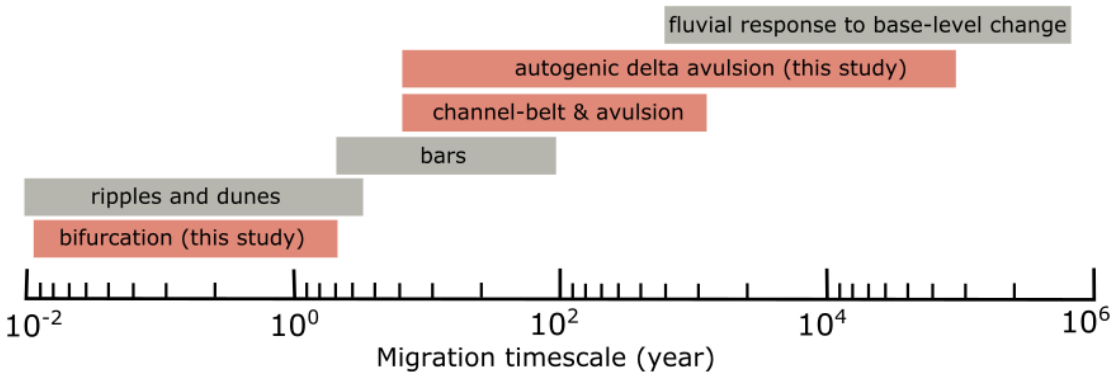

Figure 8. Autogenic and allogenic timescales from terrestrial environments (adopted from Ganti et al. (2020

Avulsions also affect preserved stratigraphy. Steeper delta topset slopes lead to more frequent avulsion and so may produce more avulsions in a given time interval (Fig. 3c). With more avulsions, increased abundance of paleosols, abandoned channel plugs, and floodplain sedimentary assemblages could be expected in the rock records. However, the preservation of evidence of autogenic signals is a function of both the timescale of this signal and the preservation potential of its stratigraphic products (Li et al., 2016; Straub et al., 2020). Evidence of autogenic signals will be preserved if either the autogenic signal timescale exceeds that of the allogenic signal (Straub et al., 2020) or the autogenically generated stratigraphic products are smaller than the autogenic reworking depth (Li et al., 2016).

In our model, the autogenic signal produced by avulsion may be autogenically reworked in the following timesteps, as shown by consistent and deep channel incisions in the upstream part of the delta (Fig. 4a). Here, the channel incised from 0-400 years during the simulation as shown in the down-dip cross section (Fig. 4a). The timescale of this autogenic reworking (0-400 years) is less than that of autogenic avulsion timescale (10^3 - 10^5 years) and hence the incision and reworking may have shredded the signal of autogenic avulsion in the preserved stratigraphy.

Future work

Our model results advance understanding about how delta topset slope controls autogenic timescale. We vary a single factor (upstream slope), although this drives and is closely correlated with upstream sediment input. The mutual adjustment of water and sediment discharge produces complex morphological and sedimentary responses. If these responses scale similarly to our results for topset slope and avulsion timescale, applying the approach used here to other autogenic forcings will reveal how deltas internally respond to these controls. Hence, our ability to disentangle autogenic and allogenic drivers will be enhanced in both modern systems and the rock record. An important extension of this work is to vary input discharge and sediment load as variability in these may affect the geomorphic processes controlling avulsion and bifurcation timescales. Multi-temporal observation of well-studied natural river deltas, such as the Yellow (Moodie et al., 2019), Mississippi (Chamberlain et al., 2018) or Rhine-Meuse (Pierik et al., 2018; Stouthamer et al., 2015), could then be used to quantify the interactions between avulsion and bifurcation that we found in our investigation.

The results from this study suggest the following areas of future study: (a) How does the autogenic forcing studied here (i.e. upstream, and the consequent topset slopes) interact with a combination of allogenic forcings (e.g. sea-level, different wave, tides, and anthropogenic effects)? (b) How do the other autogenic controls (e.g. Q_s, Q, riverbank material, vegetation) in river deltas influence avulsion timescale? How are these signals preserved or shredded in the rock record? And lastly, (c) How do seasonal or longer-term changes in input flow autogenically impact avulsion and bifurcation timescales and their interaction?

5. Conclusion

We conducted a suite of numerical modelling experiments with upstream slopes ranging from 10^{-4} to 10^{-3} to understand autogenically-controlled avulsion and bifurcation in river deltas. There is a statistically significant correlation between the topset slope produced in the model and the avulsion timescale with $T_a = 0.3{S_{topset}}^{-1.18}$; $R^2 = 69\%$, $p < 0.05$. Topset slope appears to be the dominant control of the timescale of autogenic signals, but it does not control the stratigraphy produced in the models which is remarkably consistent. Avulsion timescales span from 1.2 x 10^3 - 1.9 x 10^5 years with a median value of 1.2 x 10^4 years (N = 229). Bifurcation timescales are in the range of 2 x 10^{-2} - 5.7 x 10^1 years with a median value of 4 x 10^{-1} years (N = 201). Our findings advance understanding of how the delta topset slope serves as the first order control on autogenic timescales and how avulsion and bifurcation are not well correlated throughout the delta building process. Avulsion and bifurcation can occur at the same time during delta building, as shown by the non-unimodal distribution of dimensionless island sizes created in our model. Avulsion and bifurcation

timescale from 22 river deltas from the literature are consistent with the avulsion timescale-topset slope and bifurcation timescale-topset slope relationships proposed from our model. These findings contribute to progressing our understanding of autogenically controlled avulsion and bifurcation processes, before taking into account the influence of allogenic variables. A robust understanding of these processes has important implications due to their direct impact on coastal and inland hazards that arise from geomorphic change and flooding on highly populated river deltas.

Acknowledgements

This study was funded by an Indonesia Endowment Fund for Education (LPDP) award to Prasojo.

Open Research

The data set from natural and laboratory river deltas used in this study (Table S1 in Supporting Information) is available at https://doi.org/10.6084/m9.figshare.20654037.v1.

References

Bates, C. C. (1953). Rational Theory of Delta Formation. *AAPG Bulletin*, *37*(9), 2119–2162. https://doi.org/10.1306/5ceadd76-16bb-11d7-8645000102c1865d

Caldwell, R. L., & Edmonds, D. A. (2014). The effects of sediment properties on deltaic processes and morphologies: A numerical modeling study. *Journal of Geophysical Research: Earth Surface*, *119*(5), 961–982. https://doi.org/10.1002/2013JF002965

Cao, Q., Qingge, L., & Yang, P. (2021). Performance Analysis of Otsu-Based Thresholding Algorithms: A Comparative Study. *Journal of Sensors*, *2021*. https://doi.org/10.1155/2021/4896853

Chadwick, A. J., Lamb, M. P., & Ganti, V. (2020). Accelerated river avulsion frequency on lowland deltas due to sea-level rise. *Proceedings of the National Academy of Sciences of the United States of America*, *117*(30), 17584–17590. https://doi.org/10.1073/pnas.1912351117

Chadwick, A. J., Steele, S., Silvestre, J., & Lamb, M. P. (2022). Effect of Sea-Level Change on River Avulsions and Stratigraphy for an Experimental Lowland Delta. *Journal of Geophysical Research: Earth Surface*, *127*(7). https://doi.org/10.1029/2021JF006422

Chamberlain, E. L., Törnqvist, T. E., Shen, Z., Mauz, B., & Wallinga, J. (2018). Anatomy of Mississippi Delta growth and its implications for coastal restoration. *Science Advances*, *4*(4). https://doi.org/10.1126/SCIADV.AAR4740/SUPPL_FILE/AAR4740_SM.PDF

Chatanantavet, P., Lamb, M. P., & Nittrouer, J. A. (2012). Backwater controls of avulsion location on deltas. *Geophysical Research Letters*, *39*(1), 2–7. https://doi.org/10.1029/2011GL050197

Coleman, J. M., & Wright, L. D. (1971). *Analysis of Major River Systems and Their Deltas: Procedures and Rationale, With Two Examples*. https://apps.dtic.mil/sti/citations/AD0723575

Edmonds, D. A., Hoyal, D. C. J. D., Sheets, B. A., & Slingerland, R. L. (2009). Predicting delta avulsions: Implications for coastal wetland restoration. *Geology*, *37*(8), 759–762. https://doi.org/10.1130/G25743A.1

Edmonds, D. A., Paola, C., Hoyal, D. C. J. D., & Sheets, B. A. (2011). Quantitative metrics that describe river deltas and their channel networks. *Journal of Geophysical Research: Earth Surface*, *116*(4), 1–15. https://doi.org/10.1029/2010JF001955

Edmonds, D. A., & Slingerland, R. L. (2007). Mechanics of river mouth bar formation: Implications for the morphodynamics of delta distributary networks. *Journal of Geophysical Research: Earth Surface*, *112*(2). https://doi.org/10.1029/2006JF000574

Edmonds, D. A., & Slingerland, R. L. (2008). Stability of delta distributary networks and their bifurcations. *Water Resources Research*, *44*(9), 9426. https://doi.org/10.1029/2008WR006992

Edmonds, D. A., & Slingerland, R. L. (2010). Significant effect of sediment cohesion on deltamorphology. *Nature Geoscience*, *3*(2), 105–109. https://doi.org/10.1038/ngeo730

Ericson, J. P., Vörösmarty, C. J., Dingman, S. L., Ward, L. G., & Meybeck, M. (2006). Effective sea-level rise and deltas: Causes of change and human dimension implications. *Global and Planetary Change*, *50*(1–2), 63–82. https://doi.org/10.1016/j.gloplacha.2005.07.004

Fagherazzi, S., Edmonds, D. A., Nardin, W., Leonardi, N., Canestrelli, A., Falcini, F., Jerolmack, D. J., Mariotti, G., Rowland, J. C., & Slingerland, R. L. (2015). Dynamics of river mouth deposits. *Reviews of Geophysics*, *53*(3), 642–672. https://doi.org/10.1002/2014RG000451

Ganti, V., Chadwick, A. J., Hassenruck-Gudipati, H. J., Fuller, B. M., & Lamb, M. P. (2016). Experimental river delta size set by multiple floods and backwater hydrodynamics. *Science Advances*, *2*(5), e1501768. https://doi.org/10.1126/sciadv.1501768

Ganti, V., Chadwick, A. J., Hassenruck-Gudipati, H. J., & Lamb, M. P. (2016). Avulsion cycles and their stratigraphic signature on an experimental backwater-

controlled delta. *Journal of Geophysical Research: Earth Surface*, *121*(9), 1651–1675. https://doi.org/10.1002/2016JF003915

Ganti, V., Chu, Z., Lamb, M. P., Nittrouer, J. A., & Parker, G. (2014). Testing morphodynamic controls on the location and frequency of river avulsions on fans versus deltas: Huanghe (Yellow River), China. *Geophysical Research Letters*, *41*(22), 7882–7890. https://doi.org/10.1002/2014GL061918

Ganti, V., Hajek, E. A., Leary, K., Straub, K. M., & Paola, C. (2020). Morphodynamic Hierarchy and the Fabric of the Sedimentary Record. *Geophysical Research Letters*, *47*(14), e2020GL087921. https://doi.org/10.1029/2020GL087921

Ganti, V., Lamb, M. P., & Chadwick, A. J. (2019). Autogenic Erosional Surfaces in Fluvio-deltaic Stratigraphy from Floods, Avulsions, and Backwater Hydrodynamics. *Journal of Sedimentary Research*, *89*(8), 815–832. https://doi.org/10.2110/jsr.2019.40

Geleynse, N., Storms, J. E. A., Walstra, D. J. R., Jagers, H. R. A., Wang, Z. B., & Stive, M. J. F. (2011). Controls on river delta formation; insights from numerical modelling. *Earth and Planetary Science Letters*, *302*(1–2), 217–226. https://doi.org/10.1016/j.epsl.2010.12.013

Giosan, L., Syvitski, J., Constantinescu, S., & Day, J. (2014). Climate change: Protect the world's deltas. *Nature*, *516*(7529), 31–33. https://doi.org/10.1038/516031a

Hackney, C. R., Darby, S. E., Parsons, D. R., Leyland, J., Best, J. L., Aalto, R., Nicholas, A. P., & Houseago, R. C. (2020). River bank instability from unsustainable sand mining in the lower Mekong River. *Nature Sustainability 2020 3:3*, *3*(3), 217–225. https://doi.org/10.1038/s41893-019-0455-3

Hariharan, J., Xu, Z., Michael, H. A., Paola, C., Steel, E., & Passalacqua, P. (2021). Linking the Surface and Subsurface in River Deltas—Part 1: Relating Surface and Subsurface Geometries. *Water Resources Research*, *57*(8). https://doi.org/10.1029/2020WR029282

Heyvaert, V. M. A., & Walstra, J. (2016). The role of long-term human impact on avulsion and fan development. *Earth Surface Processes and Landforms*, *41*(14), 2137–2152. https://doi.org/10.1002/esp.4011

Hoyal, D. C. J. D., & Sheets, B. A. (2009). Morphodynamic evolution of experimental cohesive deltas. *Journal of Geophysical Research: Earth Surface*, *114*(2), 1–18. https://doi.org/10.1029/2007JF000882

Ielpi, A., & Lapôtre, M. G. A. (2019). A tenfold slowdown in river meander migration driven by plant life. *Nature Geoscience 2019 13:1*, *13*(1), 82–86. https://doi.org/10.1038/s41561-019-0491-7

Jerolmack, D. J., & Mohrig, D. (2007). Conditions for branching in depositional rives. *Geology*, *35*(5), 463–466. https://doi.org/10.1130/G23308A.1

Jerolmack, D. J., & Paola, C. (2010). Shredding of environmental signals by sediment transport. *Geophysical Research Letters*, *37*(19). https://doi.org/10.1029/2010GL044638

Jerolmack, D. J., & Swenson, J. B. (2007). Scaling relationships and evolution of distributary networks on wave-influenced deltas. *Geophysical Research Letters*, *34*(23), n/a-n/a. https://doi.org/10.1029/2007GL031823

Kleinhans, M. G. (2010). Sorting out river channel patterns. *Progress in Physical Geography*, *34*(3), 287–326. https://doi.org/10.1177/0309133310365300

Kleinhans, M. G., de Vries, B., Braat, L., & van Oorschot, M. (2018). Living landscapes: Muddy and vegetated floodplain effects on fluvial pattern in an incised river. *Earth Surface Processes and Landforms*, *43*(14), 2948–2963. https://doi.org/10.1002/ESP.4437

Kleinhans, M. G., Ferguson, R. I., Lane, S. N., & Hardy, R. J. (2013). Splitting rivers at their seams: bifurcations and avulsion. *Earth Surface Processes and Landforms*, *38*(1), 47–61. https://doi.org/10.1002/esp.3268

Kleinhans, M. G., & Hardy, R. J. (2013). River bifurcations and avulsion. In *Earth Surface Processes and Landforms* (Vol. 38, Number 3, pp. 317–318). John Wiley & Sons, Ltd. https://doi.org/10.1002/esp.3354

Kleinhans, M. G., Weerts, H. J. T., & Cohen, K. M. (2010). Avulsion in action: Reconstruction and modelling sedimentation pace and upstream flood water levels following a Medieval tidal-river diversion catastrophe (Biesbosch, The Netherlands, 1421–1750 AD). *Geomorphology*, *118*(1–2), 65–79. https://doi.org/10.1016/J.GEOMORPH.2009.12.009

Lane, E. W. (1954). *The Importance of Fluvial Morphology in Hydraulic Engineering*. https://semspub.epa.gov/work/01/554355.pdf

Leary, K. C. P., & Ganti, V. (2020). Preserved Fluvial Cross Strata Record Bedform Disequilibrium Dynamics. *Geophysical Research Letters*, *47*(2), e2019GL085910. https://doi.org/10.1029/2019GL085910

Li, J., Ganti, V., Li, C., & Wei, H. (2022). Upstream migration of avulsion sites on lowland deltas with river-mouth retreat. *Earth and Planetary Science Letters*, *577*, 117270. https://doi.org/10.1016/J.EPSL.2021.117270

Li, Q., Gasparini, N. M., & Straub, K. M. (2018). Some signals are not the same as they appear: How do erosional landscapes transform tectonic history into sediment flux records? *Geology*, *46*(5), 407–410. https://doi.org/10.1130/G40026.1

Li, Q., Yu, L., & Straub, K. M. (2016). Storage thresholds for relative sea-level signals in the stratigraphic record. *Geology*, *44*(3), 179–182. https://doi.org/10.1130/G37484.1

Loucks, D. P. (2019). Developed river deltas: are they sustainable? *Environmental Research Letters*, *14*(11), 113004. https://doi.org/10.1088/1748-9326/AB4165

Mohrig, D., Heller, P. L., Paola, C., & Lyons, W. J. (2000). Interpreting avulsion process from ancient alluvial sequences: Guadalope-Matarranya system (Northern Spain) and Wasatch formation (Western Colorado). *Bulletin of the Geological Society of America*, *112*(12), 1787–1803. https://doi.org/10.1130/0016-7606(2000)112<1787:IAPFAA>2.0.CO;2

Moodie, A. J., Nittrouer, J. A., Ma, H., Carlson, B. N., Chadwick, A. J., Lamb, M. P., & Parker, G. (2019). Modeling Deltaic Lobe-Building Cycles and Channel Avulsions for the Yellow River Delta, China. *Journal of Geophysical Research: Earth Surface*, *124*(11), 2438–2462. https://doi.org/10.1029/2019JF005220

Morgan, J. A., Kumar, N., Horner-Devine, A. R., Ahrendt, S., Istanbullouglu, E., & Bandaragoda, C. (2020). The use of a morphological acceleration factor in the simulation of large-scale fluvial morphodynamics. *Geomorphology*, *356*, 107088. https://doi.org/10.1016/J.GEOMORPH.2020.107088

Nienhuis, J. H., Hoitink, A. J. F., & Törnqvist, T. E. (2018). Future Change to Tide-Influenced Deltas. *Geophysical Research Letters*, *45*, 3499–3507. https://doi.org/doi.org/10.1029/2018GL077638

Nienhuis, J. H., Törnqvist, T. E., & Esposito, C. R. (2018). Crevasse Splays Versus Avulsions: A Recipe for Land Building With Levee Breaches. *Geophysical Research Letters*, *45*(9), 4058–4067. https://doi.org/10.1029/2018GL077933

Nijhuis, A. G., Edmonds, D. A., Caldwell, R. L., Cederberg, J. A., Slingerland, R. L., Best, J. L., Parsons, D. R., & Robinson, R. A. J. (2015). Fluvio-deltaic avulsions during relative sea-level fall. *Geology*, *43*(8), 719–722. https://doi.org/10.1130/G36788.1

Olariu, C., & Bhattacharya, J. P. (2006). Terminal distributary channels and delta front architecture of river-dominated delta systems. *Journal of Sedimentary Research*, *76*(2), 212–233. https://doi.org/10.2110/jsr.2006.026

Parker, G., Wilcock, P. R., Paola, C., Dietrich, W. E., & Pitlick, J. (2007). Physical basis for quasi-universal relations describing bankfull hydraulic geometry of single-thread gravel bed rivers. *Journal of Geophysical Research: Earth Surface*, *112*(4). https://doi.org/10.1029/2006JF000549

Pierik, H. J., Stouthamer, E., Schuring, T., & Cohen, K. M. (2018). Human-caused avulsion in the Rhine-Meuse delta before historic embankment (The Netherlands). *Geology*, *46*(11), 935–938. https://doi.org/10.1130/G45188.1

Prasojo, O. A., Hoey, T. B., Owen, A., & Williams, R. D. (2022). Slope break and avulsion locations scale consistently in global deltas. *Geophysical Research Letters*, e2021GL093656. https://doi.org/10.1029/2021GL093656

Reitz, M. D., & Jerolmack, D. J. (2012). Experimental alluvial fan evolution: Channel dynamics, slope controls, and shoreline growth. *Journal of Geophysical Research: Earth Surface*, *117*(F2), 2021. https://doi.org/10.1029/2011JF002261

Rossi, V. M., Kim, W., López, J. L., Edmonds, D., Geleynse, N.,

Olariu, C., Steel, R. J., Hiatt, M., & Passalacqua, P. (2016). Impact of tidal currents on delta-channel deepening, stratigraphic architecture, and sediment bypass beyond the shoreline. *Geology*, *44*(11), 927–930. https://doi.org/10.1130/G38334.1

Shields, M. R., Bianchi, T. S., Mohrig, D., Hutchings, J. A., Kenney, W. F., Kolker, A. S., & Curtis, J. H. (2017). Carbon storage in the Mississippi River delta enhanced by environmental engineering. *Nature Geoscience 2017 10:11*, *10*(11), 846–851. https://doi.org/10.1038/ngeo3044

Simpson, G., & Castelltort, S. (2012). Model shows that rivers transmit high-frequency climate cycles to the sedimentary record. *Geology*, *40*(12), 1131–1134. https://doi.org/10.1130/G33451.1

Slingerland, R., & Smith, N. D. (2004). River Avulsions and Their Deposits. *Annual Review of Earth and Planetary Sciences*, *32*(1), 257–285. https://doi.org/10.1146/annurev.earth.32.101802.120201

Stouthamer, E., Cohen, K. M., & Gouw, M. J. P. (2015). Avulsion and its Implications for Fluvial-Deltaic Architecture: Insights from the Holocene Rhine–Meuse Delta. *From River to Rock Record*, *97*, 215–231. https://doi.org/10.2110/sepmsp.097.215

Straub, K. M., Duller, R. A., Foreman, B. Z., & Hajek, E. A. (2020). Buffered, Incomplete, and Shredded: The Challenges of Reading an Imperfect Stratigraphic Record. *Journal of Geophysical Research: Earth Surface*, *125*(3), e2019JF005079. https://doi.org/10.1029/2019JF005079

Swenson, J. B. (2005). Relative importance of fluvial input and wave energy in controlling the timescale for distributary-channel avulsion. *Geophysical Research Letters*, *32*(23), 1–5. https://doi.org/10.1029/2005GL024758

Syvitski, J. P. M., Kettner, A. J., Overeem, I., Hutton, E. W. H., Hannon, M. T., Brakenridge, G. R., Day, J., Vörösmarty, C., Saito, Y., Giosan, L., & Nicholls, R. J. (2009). Sinking deltas due to human activities. *Nature Geoscience*, *2*(10), 681–686. https://doi.org/10.1038/ngeo629

Syvitski, J. P. M., & Saito, Y. (2007). Morphodynamics of deltas under the influence of humans. *Global and Planetary Change*, *57*(3–4), 261–282. https://doi.org/10.1016/j.gloplacha.2006.12.001

Tessler, Z. D., Vorosmarty, C. J., Grossberg, M., Gladkova, I., Aizenman, H., Syvitski, J. P. M., & Foufoula-Georgiou, E. (2015). Profiling risk and sustainability in coastal deltas of the world. *Science*, *349*, 638–643. https://doi.org/10.1126/science.aab3574

Toby, S. C., Duller, R. A., de Angelis, S., & Straub, K. M. (2019). A Stratigraphic Framework for the Preservation and Shredding of Environmental Signals. *Geophysical Research Letters*, *46*(11), 5837–5845. https://doi.org/10.1029/2019GL082555

Toby, S. C., Duller, R. A., de Angelis, S., & Straub, K. M. (2022). Morphodynamic limits to environmental signal propagation across landscapes and into strata. *Nature Communications 2022 13:1*, *13*(1), 1–10. https://doi.org/10.1038/s41467-021-27776-6

Valenza, J. M., Edmonds, D. A., Hwang, T., & Roy, S. (2020). Downstream changes in river avulsion style are related to channel morphology. *Nature Communications*, *11*(2116). https://doi.org/10.1038/s41467-020-15859-9

Wallace, D. J., Storms, J. E. A., Wallinga, J., Dam, R. L. V. A. N., Blaauw, M., Derksen, M. S., Klerks, C. J. W., Meijneken, C., Snijders, E. L. S. M. A., Fung, G., Mathematics, A., Talbot, N. L. C., Mcsherry, F., Nissim, K., Smith, A., Syvitski, J. P. M., Kettner, A. J., Overeem, I., Hutton, E. W. H., … Day, J. W. (2014). Shrinking and Sinking Deltas : Major role of Dams in delta subsidence and Effective Sea Level Rise. *Nature Geoscience*, *123*(May), 1973–1984. https://doi.org/10.1038/ngeo129

Williams, R. D., Measures, R., Hicks, D. M., & Brasington, J. (2016). Assessment of a numerical model to reproduce event-scale erosion and deposition distributions in a braided river. *Water Resources Research*, *52*(8), 6621–6642. https://doi.org/10.1002/2015WR018491

Wright, L. D. (1977). Sediment transport and deposition at river mouths: A synthesis. *Bulletin of the Geological Society of America*, *88*(6), 857–868. https://doi.org/10.1130/0016-7606(1977)88<857:STADAR>2.0.CO;2